Measurement and modeling of reverse biased electroluminescence in multi-crystalline silicon solar cells

Matthias Schneemann, Thomas Kirchartz, Reinhard Carius, and Uwe Rau

Citation: Journal of Applied Physics **114**, 134509 (2013); doi: 10.1063/1.4824099
View online: http://dx.doi.org/10.1063/1.4824099
View Table of Contents: http://scitation.aip.org/content/aip/journal/jap/114/13?ver=pdfcov
Published by the AIP Publishing

Measurement and modeling of reverse biased electroluminescence in multi-crystalline silicon solar cells

Matthias Schneemann,[1,a)] Thomas Kirchartz,[2] Reinhard Carius,[1] and Uwe Rau[1]
[1]*IEK-5-Photovoltaics, Forschungszentrum Jülich, 52425 Jülich, Germany*
[2]*Department of Physics and Centre for Plastic Electronics, Imperial College London, South Kensington Campus, London SW7 2AZ, United Kingdom*

(Received 29 July 2013; accepted 16 September 2013; published online 4 October 2013)

Calibrated microscopic measurements of electroluminescent emission spectra of reverse biased multi-crystalline silicon solar cells in a wide range of photon energies E (0.8 eV $\leq E \leq$ 4 eV) are reported. The observed spectra originating directly from point-like sources exhibit a broad maximum around 0.8 eV followed by a high photon energy tail. A model for intraband emission accurately fits microscopically measured spectra obtained from single point sources. Furthermore, we do not find significant features from interband recombination. From the fits to the intraband transition model, we extract an effective charge carrier temperature of around 4000 K for all investigated spots. The analysis also yields the different depths of the sources, which are shown to be consistent with the dimension of the space charge region. From the areas around the point sources, we observe indirect emission of internally reflected light. Due to the multiple paths through the wafer, this indirect emission exhibits a maximum at a photon energy slightly lower than the band gap energy E_g. We demonstrate that global, non-microscopic measurements are strongly influenced by this indirect radiation and therefore prone to misinterpretation. © *2013 AIP Publishing LLC*. [http://dx.doi.org/10.1063/1.4824099]

I. INTRODUCTION

Reverse biased electroluminescence (ReBEL) in silicon *p-n*-junctions is a well-known phenomenon, which has been studied mainly in the 1950s and 1960s.[1–8] More recently, the observation of ReBEL in multi crystalline silicon solar cells and the concern about the long-term stability of those devices brought the issue back into the focus of research.[9,10] Imaging of ReBEL provides additional information compared with forward biased electroluminescence (EL) imaging,[11] which is a well-established quality control tool in Si photovoltaics.[12] Forward biased EL emission is essentially homogeneous over the area of the solar cell with small variations due to locally varying minority carrier lifetimes and due to resistive and optical effects.[13] In contrast, ReBEL emerges from very small and bright spots with most of the device area being non-emissive. This bright emission under reverse bias originates from local pre-breakdown sites, which start to emit light in some cases already at applied voltages $V \approx -5$ V, and more commonly at $V \approx -12$ V. Thus, breakdown occurs in practice at much lower absolute reverse bias than expected for an ideal *p-n*-junction or solar cell with a base doping concentration $N_B = 10^{-16}$ cm^{-3} ($V = -60$ V).[14]

Intensive research in recent years led to the identification and characterization of three breakdown types in typical multi crystalline silicon solar cells, differentiated by their tangible causes in the cell. The three causes are aluminum contaminations on the surface (type 1),[15] $FeSi_2$ precipitates in grain boundaries (type 2),[16,17] and etch pits in acidic etched solar cells (type 3).[18] Since type 2 spots appear in recombination active zones, which remain dark in a forward biased EL image, these spots can easily be distinguished from types 1 and 3, which do not influence forward EL.

The excitation of the carriers is attributed to Zener tunnelling in the cases of types 1 and 2, while for the Schottky contact between $FeSi_2$ and absorber of type 2, thermionic emission[19] also plays a role.[20] Finally, for type 3 avalanche breakdown was found to happen due to the sharp etch pits. Their small tips cause edged curvatures of the *p-n*-junction which strongly increase the electrical field of the space charge region, thus significantly decreasing the breakdown voltage.[14] In the case of etch pits (type 3), avalanche multiplication factors up to four were experimentally observed.[21] All three mechanisms imply an exponential dependence of the current on the voltage drop over the breakdown site. However, this dependence is masked by the series resistance in the emitter and the base of the solar cell.[22,23]

While the research for the causes of the defect emission under reverse bias reached a satisfactory status with the characterisation of the three types,[10] there is no clear understanding of the light generation process. A key to find a proper model of the processes happening is a reliable ReBEL spectrum. The first calibrated ReBEL-spectra in *p-n*-junctions diffused and grown into silicon single crystals showed emission mainly in near infrared (NIR) with a high energy tail extending to photon energies larger than 3.3 eV.[2] This part of the spectrum makes ReBEL visible to the naked eye. Recent calibrated measurements of ReBEL in multi-crystalline silicon solar cells[22] demonstrated a spectral behaviour very similar to those earlier results. Reference 22 also showed the presence of an emission peak around the band gap energy of silicon and, additionally, demonstrated that the size of the individual emitting centres is well below the resolution limit of an optical microscope.

a)Author to whom correspondence should be addressed. Electronic mail: m.schneemann@fz-juelich.de

The present paper uses a calibrated spectral analysis of ReBEL in an extended range of wavelengths λ from $\lambda = 1600\,\text{nm}$ up to $\lambda = 300\,\text{nm}$. We show that, for all types 1–3 of breakdown sites, the measured spectra are quantitatively explained by the theory of Baraff[24] and Haecker[25] for intraband transition. Fitting the theory to our experimental data yields the temperature T^* of the hot carriers as well as the depth d_S of the emission source. Both parameters were determined in relation to spot type and onset voltage V_O for a series of breakdown sites. A distinct feature of the emission at the photon energy corresponding to the direct band gap of silicon is explained by the increase of reabsorption rather than by an increase of (interband) emission. We further find that the dominant peak at the (indirect) band gap energy measured with non-microscopic methods stems from background radiation which is not emitted from the breakdown site directly to the surface but via reflection at the back surface. This indirect radiation extends into the sub band gap energy range of Si and shows clear features of free-carrier absorption.

II. EXPERIMENT

The monochromator (Czerny-Turner-configuration) used for our experiments provides two exits, allowing the parallel use of a silicon-CCD (charge-coupled device)-camera for the visible wavelength rage and an InGaAs-PDA (photo detector array)-line-detector for the infrared, up to wavelengths $\lambda \leq 1600\,\text{nm}$. Both devices are Peltier-cooled. The spectra at energies E above $E = 3\,\text{eV}$ were measured using the second order of the monochromator grating combined with a DUG11 short-pass filter (cut off at 400 nm).

For the investigation of greater areas with diameters up to 2 mm the macroscopic setup, i.e., achromatic lenses of the adequate wavelength range are used. A higher spatial resolution is achieved with a microscope, which reduces the field of view to $Ø = 20\,\mu\text{m}$ (50× microscope objective). The typically used magnification factors are 1× ("macroscopic") and 30× ("microscopic") (Fig. 1).

For enabling comparison and interpretation of the measured data, the spectrometer was calibrated using a tungsten halogen calibration lamp. However the different properties of the calibration lamp, which is an area source and the point-like ReBEL emission complicate the correction process and require particular attention. The astigmatism of the off-axis monochromator causes a signal on the spectrometer camera, which diverges towards the edges of the detector and therefore resembles a bow tie. This is especially problematic when a detector of low height, like the InGaAs detector array, is used and the ReBEL signal outgrows the detector. For the calibration lamp, a similar issue arises for high magnifications, i.e., the use of a microscope. Therefore, it has to be ensured that the detector captures the light completely, which may require to use only the central part of the detector.

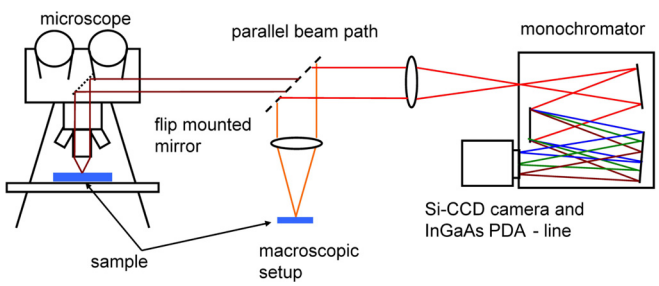

FIG. 1. Scheme of the used spectroscopy setup. The electroluminescence emission is coupled into the monochromator by an achromatic lens and finally reaches the Si CCD or InGaAs PDA detectors. Two modes may be chosen: The macroscopic setup is used for the investigation of greater areas ($Ø \approx 2\,\text{mm}$), where the field of view is defined by a lens ($f = 50\,\text{mm}$). With the microscope, the field of view can be reduced to $Ø = 20\,\mu\text{m}$.

III. THEORY

This paper uses two different models to explain the measured data theoretically. The first model assumes interband recombination between carriers that are in equilibrium with each other but not with the lattice. Let us assume recombination of pairs of these hot electrons and holes with an effective temperature T^* at a depth x underneath the surface of silicon. Then the contribution of this source at the surface of the silicon wafer is given in Boltzmann approximation by[26]

$$d\phi(E) \propto \alpha(E)\exp[-\alpha(E)x]\exp\left(\frac{-E}{k_B T^*}\right)dx, \tag{1}$$

where k_B is the Boltzmann constant. The term $\exp[-\alpha(E)x]$ takes reabsorption into account, $\alpha(E)$ is the absorption coefficient as a function of photon energy E. Integration of Eq. (1) over the radiating volume extending from d_s to $d_s+\Delta x$ yields

$$\Phi(E) \propto \{1 - \exp[-\alpha(E)\Delta x]\}\exp[-\alpha(E)d_s]\exp\left(\frac{-E}{k_B T^*}\right). \tag{2}$$

We assume the (unknown) extension of the source (Δx) to be very small, thus the term $1 - \exp[-\alpha(E)\Delta x]$ in Eq. (2) can be linearized (1st order Taylor polynomial) and the final equation used for our simulation reads

$$\Phi(E) \propto \alpha(E)\exp[-\alpha(E)d_s]\exp\left(\frac{-E}{k_B T^*}\right). \tag{3}$$

Because an absolute photon flux $\Phi(E)$ is not of interest, the only independent variables are the temperature T^* of the hot carriers (not the lattice) and the source depth d_S causing reabsorption.

The works of Baraff[24] and Haecker[25] provide the basis of the second model we use to discuss our measurements. Here, we stop using an occupation probability conceived for a quasi-equilibrium situation but take into account that a large flux of charge carriers moves parallel to a high electric field. Baraff calculates the distribution functions $f(E)$ of the accelerated carriers for energies E above and below ionization threshold E_i. For the high energy part, an analytical solution for the occupation probability can be found which reads

$$f(E) \sim (E/E_i)^{-a^*}\exp\left[-\frac{(E - E_i)}{k_B T^*}\right]. \tag{4}$$

The hot carrier temperature T^* and is used as one of the fitting parameters of this model. The exponent a^* depends on $k_B T^*$ via a quadratic equation system, that can only be solved numerically. For further details, we refer to the original paper.[24] For typical values of $k_B T^*$ determined in this study, a^* remains rather constant around $a^* = -0.23$. While no analytic solution can be written down for the distribution function for energies below threshold E_i, the numeric calculation is straight forward and again shown in Baraff's work.[24]

Haecker takes the above distribution functions and applies them to direct intraband transitions of hot holes (no interband electron-hole-recombination). If we use Haecker's solution for the emission and multiply it with the same reabsorption term as used in Eq. (2), we obtain

$$\Phi(E) \sim E^{3.5} f[E/(1 - m_1/m_2)] \exp[-\alpha(E) d_S]. \qquad (5)$$

In silicon, the ratio of the effective masses m_1 and m_2 of the light and heavy hole bands is $m_1/m_2 = 0.29$.[25] Further required constants are the energy loss per hole collision $E_r = 63\,\text{meV}$[25] and the mean free path for ionizing collisions l_i and the mean free path $\lambda_R = 7.6\,\text{nm}$[25] for collisions loosing energy to phonons. We assume l_i to be three times[27] as long as λ_R, while the actual value has no significant influence on the outcome of the simulations.

IV. RESULTS

A. Analysis of an individual type 1 spot

Fig. 2 shows a microscopic spectrum of type 1-ReBEL from NIR to VIS, measured with the InGaAs-PDA and the Si-CCD, respectively. In the UV energy range ($E \geq 3\,\text{eV}$), the microscope optics show fluorescence and stray light, so only the macroscopic setup with UV-grade quartz lenses could be used. However, comparisons of microscopic and macroscopic measurements show no differences in the VIS range ($1.4\,\text{eV} \leq E \leq 3\,\text{eV}$). We therefore assume that the macroscopic measurements are also consistent with microscopic measurements for higher photon energies E.

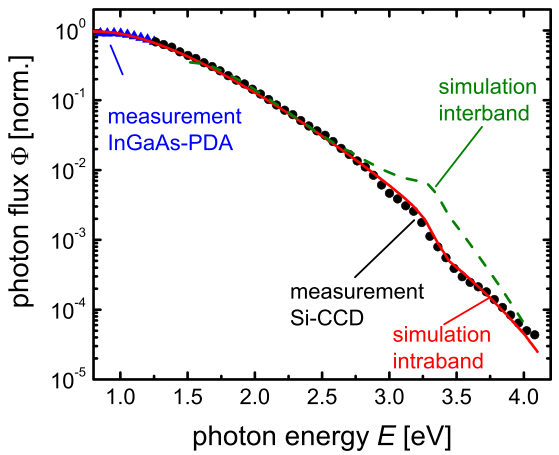

FIG. 2. Combined ReBEL-spectra of a type 1 spot, measured with InGaAs PDA (blue triangles) and Silicon CCD (black circles). The measured curve shows a continuously decreasing course towards the UV, featuring a slight kink at the direct band gap energy $E_{dg,1} = 3.4\,\text{eV}$. A comparison of the measured spectrum with the modeled intraband transitions shows a very good agreement over the entire energy range. Contrarily, the interband recombination model shows a distinct shoulder at the direct band gap energy, which is not found in the measurement.

The curve has its maximum at the low energy end of our measurement range, where however the gradient is still smaller than zero, i.e., the global peak of the spectrum is probably at smaller photon energies. Since there is significant emission at energies below the smallest, indirect band gap energy of silicon, the radiating transitions take place within the valence- or conduction bands, respectively (intraband transitions).

In the visible range, the spectrum follows an almost exponential path with a slight curvature in this semi logarithmic plot, until it reaches the ultraviolet, where silicon has two direct bandgaps ($E_{dg,1} = 3.4\,\text{eV}$, $E_{dg,2} = 4.2\,\text{eV}$).[28] However instead of showing an increase or a shoulder at the direct bandgaps, the spectrum even decays faster around 3.3 eV. Especially, this feature will now be discussed with both models described above.

In Fig. 2, the measured curve is firstly compared with a calculated Baraff-Haecker-fit [Eq. (5), solid red line in Fig. 2] and shows a very good agreement over the entire measurement range. The used intraband model is not affected by the direct band gaps and therefore does not produce an increased emission at the corresponding energy. Instead, a shallow source depth $d_S = 9\,\text{nm}$ reproduces the reabsorption kink at the direct band gap energy perfectly and the temperature T^* of the hot holes amounts to $T^* = 3550\,\text{K}$. According to Haecker,[25] the threshold energy E_i is estimated to be in the range $E_g \leq E_i \leq 1.5\,E_g$. In the present case, the best fit to the infrared region of our measurement is achieved for $E_i = E_g$.

In principle, also interband recombination [Eq. (3), dashed green line in Fig. 2, $T^* = 1850\,\text{K}$, $d_S = 9\,\text{nm}$] can be applied to the high energy region of the spectrum. However, the strong rise of the absorption coefficient $\alpha(E)$ at the direct band gaps of silicon causes on one hand an increase of the emission, and on the other hand also a strong increase of the reabsorption. To reproduce the measured data, both effects would have to be balanced out. We found out that this would only be possible, if the term $1 - \exp[-\alpha(E)\Delta x]$ in Eq. (2) was already in saturation due to a long length Δx of the radiating volume. Our calculations show that a length $\Delta x > 200\,\text{nm}$ would be required. Taking the width w of the space charge region as an upper limit of Δx, smaller numbers are expected.

The presented type 1 spot is caused by a Zener junction between the n-emitter and the region below the aluminum contamination, which are both highly doped. The width of the space charge regions of such devices is on the order of $w = 40\,\text{nm}$.[29] Therefore, we conclude from our data that ReBEL emission is caused only by intraband transitions and interband transition between conduction and valence band does not play a significant role.

B. Analysis of individual spots of types 2 and 3

In Sec. IV B, the parameters temperature T^* of the hot holes as well as the source depth d_S are investigated regarding

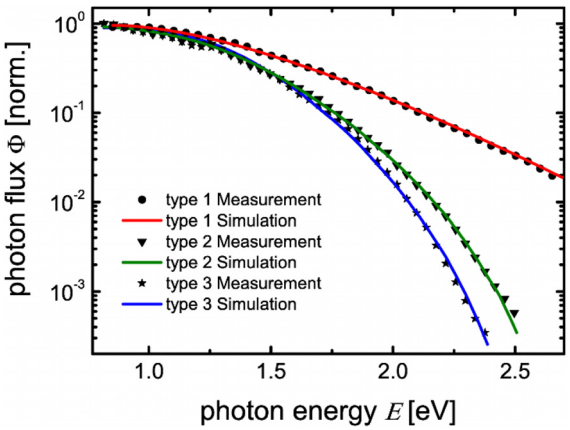

FIG. 3. Individual spectra and respective fits of individual breakdown sites corresponding to the three spot types 1–3, measured at the same acidic etched mc-Si solar cell with an applied voltage $V = 16$ V. The data are normalized and fit parameters given in Table I.

spot type and onset voltage V_O. The Baraff-Haecker-Model will be used to fit the measured spectra.

Fig. 3 shows exemplary microscope spectra for each spot type appearing on the very same acidic etched mc-Si solar cell. The light emitted by the type 1 spot has by far the highest relative share of visible light, exceeding the photon flux of the other two types by a factor of 100 at the high energy end of the measurement ($E = 2.5$ eV). Using the Baraff-Haecker-approach, the three spectra were modelled and fitted with results shown in Table I and Fig. 3. The difference between the three spectra is mainly due to different defect depths d_S. In contrast to type 1, the other types are located deeper below the surface at $d_S \approx 4\,\mu$m. The hot carriers of all types have fairly similar temperatures $T^* = 3660\,\text{K} \pm 5\%$. Note that only the source depth d_S, i.e., reabsorption is responsible for the bigger curvature of the spectra of deeper origin, while the temperature T^* only changes the slope over the entire VIS-UV-range. Each set of d_S and T^* has an error of about $\Delta d_S = \pm\ 0.2\,\mu$m and $\Delta T^* = \pm\ 200$ K.

C. Onset voltage

The onset voltage V_O is defined as the smallest applied voltage causing the respective defect to emit light. As another important distinguishing feature of a ReBEL spot besides the spot type, the influence of the onset voltage V_O on the parameters temperature T^* and source depths d_S will be investigated in the following. We present a type 2 spot series originating from an alkaline etched mc-Si solar cell and a type 3 spot series from an acidic etched mc-Si solar cell. Measurement and analysis of the ReBEL spectra were carried out as above, but only the results for the temperature T^* and the source depth d_s will be displayed in the following.

As shown in Fig. 4, the temperatures T^* of this series are in the same range as those above and are distributed quite closely around $T = 4100\,\text{K} \pm 14\%$. Furthermore, the measured defect depths d_S are small compared with the thickness $d \approx 200\,\mu$m of the solar cell and are calculated to be $1.9\,\mu\text{m} \leq d_S \leq 3.2\,\mu$m (type 2) or $2.3\,\mu\text{m} \leq d_S \leq 7.2\,\mu$m (type 3). This result corresponds well to the dimension of the space charge region at the applied voltages $-18\,\text{V} \leq V \leq -10\,\text{V}$. This conclusion requires a consideration of the etched surface features and therefore both alkaline- and acidic surface textures are discussed in the following segment.

The height of a surface feature of a solar cell can be measured under a microscope by shifting the focal plane of the instrument. For acidic etched solar cells, height differences of the surface structure of more than $10\,\mu$m are found, while the lateral sizes are in the sub micrometer range. Therefore, the escaping ReBEL light travels partly through air and silicon and the measured source depth d_S must be understood as an effective result. Contrarily, the measured source depths d_S of alkaline textured solar cells can be taken as the actual distance from the surface, because the surface features are usually much bigger than the ReBEL spot size. However, their surface is covered with pyramids. The emitter is diffused conformally as is therefore also the space charge region [inset in Fig. 4(a)]. On its way to the surface, the ReBEL emission has to cross the space charge region diagonally, whose effective thickness d_{eff} is therefore

TABLE I. Fit parameters for the reproduction of the measured spectra of the three spot types depicted in Fig. 3.

	Temperature T [K]	Source depth d_S [μm]
Type 1	3800	0.01
Type 2	3500	3.5
Type 3	3700	3.8

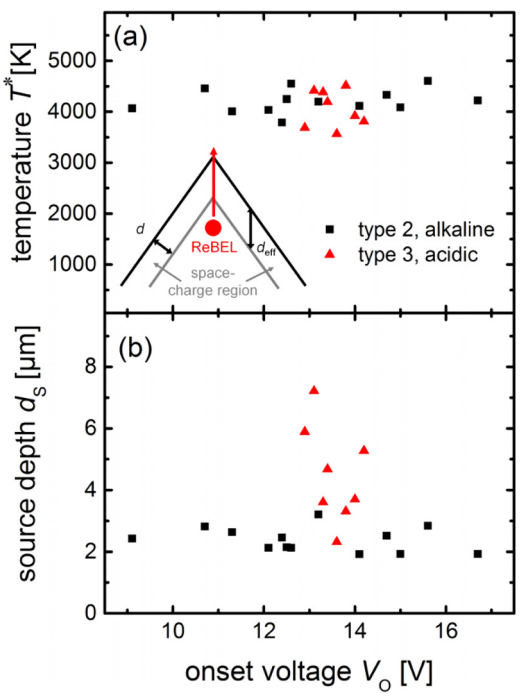

FIG. 4. (a) For the presented type 2 and type 3 series (alkaline and acidic texture, respectively), typical values for the temperature T^* of the hot carriers are close to $T^* = 4100\,\text{K} \pm 14\%$. (b) The values of the source depth d_S of the individual type 2 (black squares) spot accumulate around $d_S = 2.4\,\mu$m, while the type 3 (red triangles) shows diverse source depth in the range $2.3 \leq d_S \leq 7.2\,\mu$m. The inset in (a) sketches the effective dimension of the space charge region for alkaline textured solar cells.

increased. With this consideration, we find that the calculated source depths d_S are located in the space charge region.

The differences of the spectra of all ReBEL spots are mainly due to different source depths and small variations of the temperature of the hot carriers. We therefore conclude that the light generation process can be modeled with an intraband transition ansatz and is always the same, disregarding the generation process of the hot carriers.

D. Indirect radiation due to internal reflections

Our microscopically measured ReBEL spectra exhibit a maximum at 0.8 eV (Fig. 4). This is in conflict to earlier work,[7,22,25,30,31] where a peak of the emission at the band gap energy of silicon was reported. This finding led to the conclusion that interband recombination plays an important role at least in this spectral range.

However, all these results were obtained with integral measurements and cannot distinguish between radiation that originates directly from the spot and possible indirect radiation that could, in the spectral range of low absorption of silicon, also stem from light that is first reflected at the back contact before it is emitted at the front surface.

Fig. 5 shows microscopic (10× NIR lens) ReBEL images of the three spot types taken with a 16 bit peltier-cooled InGaAs-PDA-camera, having a sensitivity range extending from 0.75 to 1.3 eV. For the type 1 spot (a), we see that there is a halo-like emission with a radius of about 100 μm in the vicinity of the direct emission. The ReBEL-spots are about three orders of magnitude more intense than the indirect emission. Nevertheless, the indirect emission visualizes clearly the surface structure of the cells, i.e., the "carpet pattern" of the acidic etched cells (a,c) and pyramids of the alkaline etched cell (b). Though the signal-to-noise-ratio is not satisfying, we may estimate the integral intensities of direct and indirect emission to be the same.

Fig. 6(a) shows the spectrum of the background emission, which was measured around a type 1 spot under a microscope, while the main emission was covered with an acuminated wire (see inset). The background spectrum rises strongly at $E = 1.2$ eV and reaches its maximum at the band gap energy of silicon. Afterwards, the intensity decreases slowly towards the infrared end of the measurement range. The red curve in Fig. 6(a) is obtained from a macroscopic FTIR measurement of the complete type 1 emission using an extended InGaAs-detector. The "dark field" spectrum (with wire) and the global, macroscopically measured spectrum are equal in the range of 0.8–1.2 eV showing that the macroscopic measurement is dominated by the indirect emission. The spectrum of the direct emission is also plotted for comparison.

Fig. 6(b) shows the absorptance of a fragment of the same acidic etched mc-Si solar cell on which the type 1 spot is found. The absorptance is measured using a photothermal deflection spectroscopy (PDS) setup.[32] The absorption is reduced for energies below the band gap energy and the free carrier absorption of the doped wafer[33] increases continuously towards low photon energies. The indirect emission spectra in Fig. 6(a) resemble a mirror image of the absorptance of the cell, which indicates that the indirect emission spectrum obtains its shape, i.e., its maximum from a decrease of reabsorption by the wafer rather than from an increase of emission. The indirect light has therefore travelled a long way through the wafer, losing all photons with energies that are absorbed significantly in silicon. We suggest that the indirect emission is regular ReBEL, which is both reflected at the surface and emitted towards the bottom of the solar cell where it is reflected back to the surface. Part of the light then leaves the device as sketched in the inset of Fig. 6 and contributes to the macroscopic ReBEL spectra.

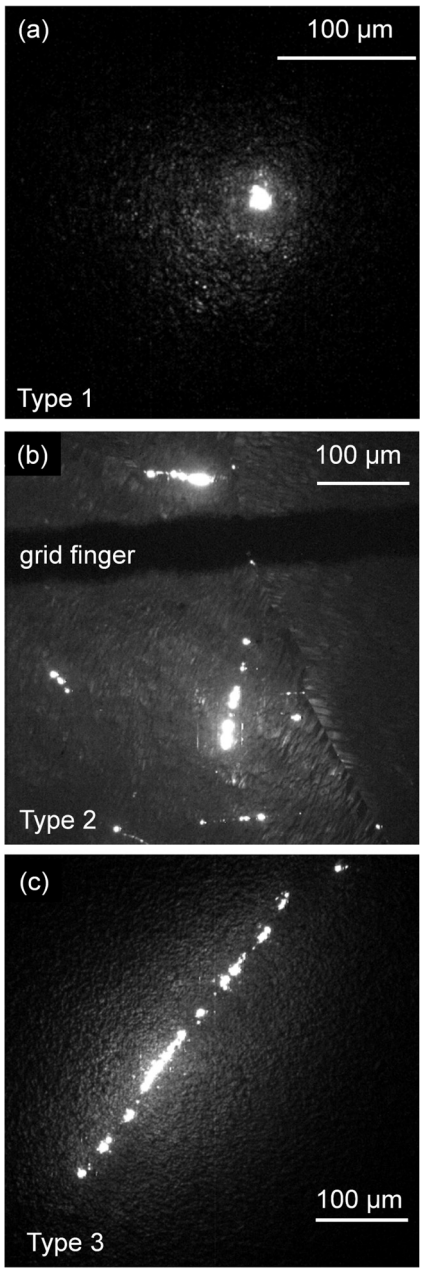

FIG. 5. Microscopic ReBEL images of (a) a type 1 spot, (b) type 2, and (c) type 3 spot with strongly enhanced contrast. Besides the well-known spot-like emission, we find a wide halo-like emission around the spots. The indirect radiation is about three orders of magnitude weaker than the spots. To achieve a reasonable signal to noise ratio for these pictures, the direct emission (spots) was overexposed by a factor of ten and one hundred images were combined.

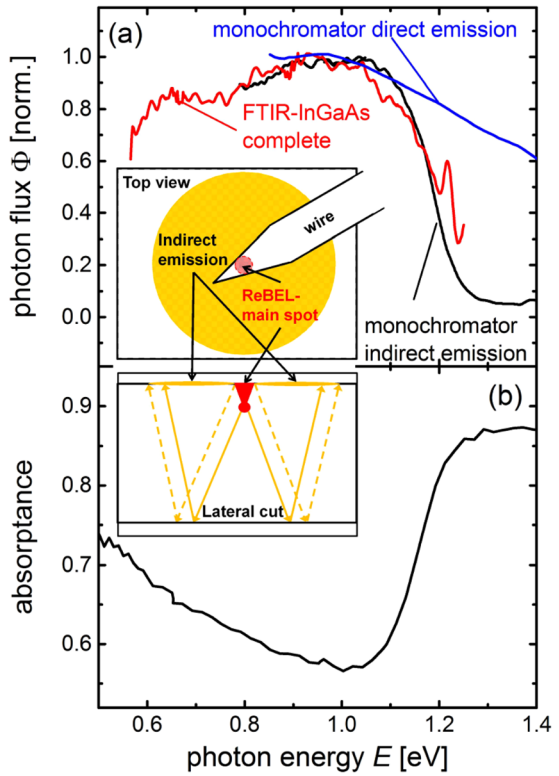

FIG. 6. (a) Spectrum of the ReBEL background radiation measured with a monochromator-system. A strong increase of the emission is seen around the band gap energy of silicon $E_g = 1.1$ eV, which corresponds well with the decrease of the absorptance of the cell which was measured with PDS (b). Furthermore, the background radiation spectrum and the non-microscopic ReBEL measurement of a FTIR (including ReBEL main spot and background emission) resemble each other. The inset describes the extraction of the background radiation by shadowing the bright point-like emission with a wire and the suggested propagation of the indirect emission through the cell.

V. CONCLUSION

The extended spectral measurement range achieved in this work allows reliable conclusions about the light generation processes of the reversed biased electroluminescence of multi-crystalline Si solar cells. We detected infrared radiation at photon energies below the smallest band gap of silicon at $E_g = 1.12$ eV and no sign of increased emission at the direct band gaps of silicon in the ultraviolet ($E_{dg,1} = 3.4$ eV and $E_{dg,2} = 4.2$ eV). Both facts are strong arguments against interband recombination and favour intraband transitions of hot holes and/or hot electrons, at least in the mentioned energy ranges $E < 1.12$ eV and around $E \approx 3.4$ eV and $E \approx 4.2$ eV. The intraband model of Baraff and Haecker[24,25] yields a good fit to measured spectra over the complete measurement range.

Numerous ReBEL spots were investigated and evaluated with the Baraff-Haecker-model with respect to their spot type, surface texture and their onset voltage V_O. All spots exhibit a similar temperature T^* of the hot carriers and the depths of the sources is found to be in the space charge region, when the surface features of the respective cells are accounted for.

Internal reflections of inward emitted light cause an indirect, halo-like luminescence around the point-like ReBEL spots. The indirect intensity is weaker by three orders of magnitude than the direct emission. Nevertheless, if spectroscopy is conducted non-microscopically, the indirect emission causes increased relative intensities at energies around the indirect band gap of silicon.

ACKNOWLEDGMENTS

The authors want to thank Jan Flohre, Josef Klomfass, Markus Hülsbeck, and Urs Aeberhard for help with the experiments and fruitful discussions. T.K. acknowledges support by an Imperial College Junior Research Fellowship.

[1]R. Newman, Phys. Rev. **100**, 700 (1955).
[2]A. G. Chynoweth and K. G. McKay, Phys. Rev. **102**, 369 (1956).
[3]A. Goetzberger and W. Shockley, J. Appl. Phys. **31**, 1821 (1960).
[4]W. Shockley, Solid-State Electron. **2**, 35 (1961).
[5]S. Mahadevan, S. M. Hardas, and G. Suryan, Phys. Status Solidi A **8**, 335 (1971).
[6]T. Figielski and A. Torun, in *Proceedings of the International Conference on the Physics of Semiconductors*, Exeter, UK (The Institute of Physics, London, 1962), p. 863.
[7]A. L. Lacaita, F. Zappa, S. Bigliardi, and M. Manfredi, IEEE Trans. Electron Devices **40**, 577 (1993).
[8]J. Bude, N. Sano, and A. Yoshii, Phys. Rev. B **45**, 5848 (1992).
[9]Y. Kaji, H. Kondo, Y. Takahashi, T. Yamazaki, Y. Uraoka, and T. Fuyuki, in *Proceedings of the 31st IEEE Photovoltaic Specialists Conference, Orlando* (IEEE, Piscataway, NJ, 2005), pp. 1346–1348.
[10]O. Breitenstein, J. Bauer, K. Bothe, W. Kwapil, D. Lausch, U. Rau, J. Schmidt, M. Schneemann, M. C. Schubert, J.-M. Wagner, and W. Warta, J. Appl. Phys. **109**, 071101 (2011).
[11]T. Fuyuki, H. Kondo, T. Yamazaki, Y. Takahashi, and Y. Uraoka, Appl. Phys. Lett. **86**, 262108 (2005).
[12]T. Trupke, J. Nyhus, and J. Haunschild, Phys. Status Solidi RRL **5**, 131–137 (2011).
[13]T. Kirchartz, A. Helbig, W. Reetz, M. Reuter, J. H. Werner, and U. Rau, Prog. Photovoltaics **17**, 394 (2009).
[14]S. M. Sze and G. Gibbons, Solid-State Electron. **9**, 831 (1966).
[15]D. Lausch, K. Petter, R. Bakowski, C. Czekalla, J. Lenzner, H. V. Wenckstern, and M. Grundmann, Appl. Phys. Lett. **97**, 073506 (2010).
[16]W. Kwapil, P. Gundel, M. C. Schubert, F. D. Heinz, W. Warta, E. R. Weber, A. Goetzberger, and G. Martinez-Criado, Appl. Phys. Lett. **95**, 232113 (2009).
[17]A. Haehnel, J. Bauer, H. Blumtritt, O. Breitenstein, D. Lausch, and W. Kwapil, J. Appl. Phys. **113**, 044505 (2013).
[18]J. Bauer, J. M. Wagner, A. Lotnyk, H. Blumtritt, B. Lim, J. Schmidt, and O. Breitenstein, Phys. Status Solidi RRL **3**, 40 (2009).
[19]E. H. Rhoderick, *Metal-Semiconductor Contacts, Conference Series* (Institute of Physics, London, 1974), Vol. 22, p. 3.
[20]*Handbook on Semiconductors Volume 4, Device Physics*, edited by C. Hilsum (North-Holland, 1985).
[21]O. Breitenstein, J. Bauer, J.-M. Wagner, and A. Lotnyk, Prog. Photovoltaics **16**, 679 (2008).
[22]M. Schneemann, A. Helbig, T. Kirchartz, R. Carius, and U. Rau, Phys. Status Solidi A **207**, 2597 (2010).
[23]M. Schneemann, A. Helbig, T. Kirchartz, R. Carius, and U. Rau, in 25th European Photovoltaic Solar Energy Conference and Exhibition, Valencia, Spain, 2010.
[24]G. A. Baraff, Phys. Rev. **133**, A26 (1964).
[25]W. Haecker, Phys. Status Solidi A **25**, 301 (1974).
[26]W. van Roosbroeck and W. Shockley, Phys. Rev. **94**, 1558 (1954).
[27]D. J. Bartelink, J. L. Moll, and N. I. Meyer, Phys. Rev. **130**, 972 (1963).
[28]J. R. Chelikowsky and M. L. Cohen, Phys. Rev. B **10**, 5095 (1974).
[29]S. M. Sze and K. N. G. Kwok, *Physics of Semiconductor Devices* (Wiley, 2007).
[30]N. C. Das and B. M. Arora, Appl. Phys. Lett. **56**, 1152 (1990).
[31]M. Herzog and F. Koch, Appl. Phys. Lett. **53**, 2620 (1988).
[32]W. B. Jackson, N. M. Amer, A. C. Boccara, and D. Fournier, Appl. Optics **20**, 1333 (1981).
[33]D. K. Schroder, R. N. Thomas, and J. C. Swartz, IEEE J. Solid-State Circuits **13**, 180 (1978).